bioRxiv preprint doi: https://doi.org/10.1101/106955; this version posted April 5, 2017. The copyright holder for this preprint (which was not certified by peer review) is the author/funder. All rights reserved. No reuse allowed without permission.

Recent Regulatory Changes Shaped Human Facial and Vocal Anatomy

David Gokhman[1], Lily Agranat-Tamir[1,2], Genevieve Housman[3,4], Raquel García-Pérez[5], Malka Nissim-Rafinia[1], Swapan Mallick[6,7,8], Maria A. Nieves-Colón[3,4], Hongcang Gu[6], Manuel Ferrando-Bernal[5], Pere Gelabert[5], Iddi Lipende[9], Ivanela Kondova[10], Ronald Bontrop[10], Ellen E. Quillen[11], Alexander Meissner[6,12,13], Anne C. Stone[3,4,14], Anne E. Pusey[15], Deus Mjungu[9], Leonid Kandel[16], Meir Liebergall[16], María E. Prada[17], Julio M. Vidal[18], Kay Prüfer[19], Johannes Krause[20], Benjamin Yakir[2], Svante Pääbo[19], David Reich[6,7,8], Carles Lalueza-Fox[5], Tomas Marques-Bonet[5,21,22], Eran Meshorer[1,23,*], Liran Carmel[1,*]

[1] Department of Genetics, The Alexander Silberman Institute of Life Sciences, Faculty of Science, The Hebrew University of Jerusalem, Edmond J. Safra Campus, Givat Ram, Jerusalem 91904, Israel.
[2] Department of Statistics, The Hebrew University of Jerusalem, Jerusalem 91905, Israel.
[3] School of Human Evolution and Social Change, Arizona State University, Tempe, AZ 85281, USA.
[4] Center for Evolution and Medicine, Arizona State University, Tempe, AZ 85287, USA.
[5] Institute of Evolutionary Biology (UPF-CSIC), 08003 Barcelona, Spain.
[6] Broad Institute, Cambridge MA 02138, USA.
[7] Department of Genetics, Harvard Medical School, Boston, MA 02115, USA.
[8] Howard Hughes Medical Institute, Harvard Medical School, Boston, MA 02115, USA.
[9] Gombe Stream Research Center, Jane Goodall Institute, Kigoma, Tanzania.
[10] Biomedical Primate Research Center (BPRC), Rijswijk, The Netherlands.
[11] Department of Genetics, Texas Biomedical Research Institute, San Antonio, Texas 85287, USA.
[12] Harvard Stem Cell Institute, Cambridge, MA 02138 USA.
[13] Department of Stem Cell and Regenerative Biology, Harvard University, Cambridge, MA 02138 USA
[14] Institute of Human Origins, Arizona State University, Tempe, AZ 85287, USA.
[15] Department of Evolutionary Anthropology , Duke University , Durham, NC 27708, USA.
[16] Orthopaedic Department, Hadassah – Hebrew University Medical Center, Jerusalem, Israel.
[17] I.E.S.O. 'Los Salados'. Junta de Castilla y León, Spain.
[18] Junta de Castilla y León, Servicio de Cultura de León, Spain.
[19] Department of Evolutionary Genetics, Max Planck Institute for Evolutionary Anthropology, Leipzig D-04103, Germany.
[20] Max Planck Institute for the Science of Human History, 07745 Jena, Germany.
[21] Catalan Institution of Research and Advanced Studies (ICREA), 08010 Barcelona, Spain.
[22] Centro Nacional de Análisis Genómico (CRG-CNAG), 08028 Barcelona, Spain.
[23] The Edmond and Lily Safra Center for Brain Sciences (ELSC), The Hebrew University of Jerusalem, Edmond J. Safra Campus, Givat Ram, Jerusalem, 91904, Israel.

bioRxiv preprint doi: https://doi.org/10.1101/106955; this version posted April 5, 2017. The copyright holder for this preprint (which was not certified by peer review) is the author/funder. All rights reserved. No reuse allowed without permission.

Identifying changes in gene regulation that shaped human-specific traits is critical to understanding human evolution. Here, we use >60 DNA methylation maps of different human groups, both present-day and ancient, as well as six chimpanzee maps, to detect regulatory changes that emerged specifically in modern humans. We show that genes affecting vocalization and facial features went through particularly extensive changes in methylation. Especially, we identify expansive changes in a network of genes regulating skeletal development (*SOX9*, *ACAN* and *COL2A1*), and in *NFIX*, which controls facial projection and voice box (larynx) development. We propose that these changes might have played a key role in shaping the human face, and in forming the human 1:1 vocal tract configuration that is considered optimal for speech. Our results provide insights into the molecular mechanisms that underlie modern human face and voice, and suggest that they arose after the split from Neanderthals and Denisovans.

bioRxiv preprint doi: https://doi.org/10.1101/106955; this version posted April 5, 2017. The copyright holder for this preprint (which was not certified by peer review) is the author/funder. All rights reserved. No reuse allowed without permission.

The advent of high-quality ancient genomes of archaic humans (Neanderthal and Denisovan) opened up the possibility to identify the genetic basis of some unique modern human traits[1,2]. A common approach is to carry out sequence comparisons and identify non-neutral sequence changes. However, out of ~30,000 fixed substitutions and indels that reached fixation on the lineage of present-day humans after their separation from archaic humans, only ~100 directly alter amino acid sequence[1], and as of today our ability to estimate the biological effect of the rest of these changes is limited. While most of these sequence changes are probably nearly neutral, some may affect gene function, especially those in regulatory regions such as promoters and enhancers. Such regulatory changes may have sizeable impact on human evolution, as alterations in gene regulation are thought to account for much of the phenotypic variation between closely related groups[3]. Thus, direct examination of DNA regulatory layers such as DNA methylation is critical in understanding human-specific traits.

A key trait that sets humans apart from other apes is our unique ability to communicate through speech. This capacity is attributed not only to neural changes, but also to structural alterations to the vocal tract[4,5]. The relative role of anatomy in our speech skills is still debated[4,6], but it is nevertheless widely accepted that even with a human brain, other apes could not reach the human level of articulation[4,5]. Non-human apes are restricted not only in their linguistic capacity (e.g., they can hardly learn grammar[5]), but also in their ability to produce the phonetic range that humans can. Indeed, chimpanzees communicate through sign language and symbols much better than they do vocally, even after being raised in an entirely human environment[5]. Phonetic range is determined by the different conformations that the vocal tract can produce. These conformations are largely shaped by the position of the larynx, tongue, lips and mandible. Modern humans have a 1:1 proportion between the horizontal and vertical dimensions of the vocal tract, which is unique among primates[4,7] (Fig. 1a). It is still debated whether this configuration is a prerequisite for speech, but it was nonetheless shown to be optimal for speech[4,5,7–9]. The 1:1 proportion was reached through a relative shortening of the human face, together with the descent of the larynx[10]. Attempts to use anthropological remains to determine whether Neanderthals and modern humans share similar vocal anatomy proved hard, as cartilaginous tissues do not survive long after death and the only remnant from the Neanderthal laryngeal region is the hyoid bone[511]. Based on this single bone, or on computer simulations and tentative vocal tract reconstructions, it is difficult to

bioRxiv preprint doi: https://doi.org/10.1101/106955; this version posted April 5, 2017. The copyright holder for this preprint (which was not certified by peer review) is the author/funder. All rights reserved. No reuse allowed without permission.

characterize the full anatomy of the Neanderthal vocal apparatus, and opinions remain split as to whether it was similar to modern humans[5,11,12].

To gain insight into the genetic regulation that underlies human evolution, we have previously developed a method to reconstruct pre-mortem DNA methylation maps of ancient genomes[13] based on analysis of patterns of damage to ancient DNA[13–15]. We have used this method to reconstruct the methylomes of a Neanderthal and a Denisovan, and compared them to a present-day osteoblast methylation map[13]. However, the ability to identify differentially methylated regions (DMRs) between the human groups was confined by the incomplete reference map, the differences in sequencing technologies, the lack of an outgroup and the restricted set of skeletal samples (see Methods). Here, we sought to identify DMRs based on a comprehensive assembly of skeletal DNA methylation maps. To the previously reconstructed Denisovan and Altai Neanderthal methylation maps, we added the methylome of the ~40,000 years old (yo) Vindija Neanderthal, and four methylomes of anatomically modern humans: the ~45,000 yo Ust'-Ishim indvidual[16], the ~8,000 yo Loschbour individual[17], the ~7,000 yo Stuttgart individual[17], and the ~7,000 yo La Braña 1 individual[18] whose genome we sequenced to high-coverage. To obtain full present-day maps, we produced whole-genome bisulfite sequencing (WGBS) methylomes from the femur bones of two present-day individuals (hereinafter, Bone1 and Bone2). To this we added 54 publically available partial bone methylation maps from present-day individuals, produced using reduced-representation bisulfite-sequencing (RRBS)[19] and 450K methylation arrays[20,21]. Hereinafter, ancient and present-day modern humans are collectively referred to as *modern humans* (MHs), while the Neanderthal and Denisovan are referred to as *archaic humans*. As an outgroup, we produced methylomes from six chimpanzees (WGBS, RRBS, and four 850K methylation arrays; Extended Data Table 1). Together, these data establish a unique and comprehensive platform to study DNA methylation dynamics in recent human evolution.

Identifying DMRs

In order to minimize artifacts that might arise from comparing methylation maps produced through different technologies, we used the reconstructed Ust'-Ishim methylome as the MH reference, to which we compared the Altai Neanderthal and the Denisovan. We identified 18,080 loci that showed methylation differences between these individuals. Notably, these DMRs do not necessarily represent differences between the human groups. Rather, many of them could be

bioRxiv preprint doi: https://doi.org/10.1101/106955; this version posted April 5, 2017. The copyright holder for this preprint (which was not certified by peer review) is the author/funder. All rights reserved. No reuse allowed without permission.

attributed to factors separating the three individuals (e.g., Ust'-Ishim is a male whereas the archaic humans are females), or to variability within populations. To account for this, we used the ~50 additional human maps to filter out regions where variability in methylation is detected. Importantly, our samples come from both sexes, from individuals of various ages and ancestries, and from a variety of skeletal parts (tooth, femur, phalanx, rib; Extended Data Table 1), hence allowing the removal of DMRs that might arise due to any of these variables. This left a set of 6,371 DMRs that discriminate between the human groups, which we ranked according to their significance level (Extended Data Table 2).

Next, using the chimpanzee samples, we were able to determine for 3,869 of these DMRs the lineage where the methylation change occurred. Of these DMRs 1,667 were MH-derived, 1,103 were archaic-derived, 597 were Neanderthal-derived, and 502 were Denisovan-derived (Fig. 1b). The large number of MH samples used to filter out within population variability led us to focus in this work on MH-derived DMRs. We assigned them to three hierarchies based on which samples were used to filter out variable loci: (i) The list of 1,667 DMRs was derived using all full (WGBS and reconstructed) MH and chimpanzee bone methylomes (hereinafter, full bone MH-derived). (ii) For 1,100 DMRs we also had information from the partial (450K and 850K methylation arrays) MH and chimpanzee bone methylomes (hereinafter, bone MH-derived). (iii) For 881 DMRs we used information from all MH and chimpanzee skeletal methylomes, including teeth (hereinafter, skeletal MH-derived, Extended Data Table 2).

Voice-affecting genes are derived in MHs

We defined differentially methylated genes (DMGs) as genes that overlap at least one DMR along their body or up to a distance of 5 kb upstream (Extended Data Table 2). To gain insight into the function of these DMGs, we analyzed their gene ontology. As expected from a comparison between skeletal tissues, all three hierarchies of MH-derived DMGs are enriched with terms associated with the skeleton (e.g., *chondrocyte differentiation*, *proteoglycan biosynthetic process*, *cartilage development*, *embryonic skeletal system development* and *ossification*). Also notable are terms associated with the skeletal muscle, cardiovascular and nervous system (Extended Data Table 3).

To get a more precise picture of the possible functional consequences of these DMGs, we used Gene ORGANizer[22] (geneorganizer.huji.ac.il). This is a tool that links genes to the organs where

bioRxiv preprint doi: https://doi.org/10.1101/106955; this version posted April 5, 2017. The copyright holder for this preprint (which was not certified by peer review) is the author/funder. All rights reserved. No reuse allowed without permission.

their phenotypes are observed, and was built based on curated gene-disease and gene-phenotype associations. We used Gene ORGANizer to identify body parts that are significantly over-represented in our DMG lists. We found that within MH-derived DMGs, genes that affect the voice are the most enriched (Fig. 1c, Extended Data Table 4). For example, when running the list of skeletal MH-derived DMRs, we identified 14 significantly enriched body parts, with the strongest enrichment in the vocal cords (x2.18, FDR = 0.01), followed by the voice box (larynx, x1.74, FDR = 0.029) and then by body parts belonging primarily to the face, spine and pelvis. Interestingly, these parts are considered to be among the most morphologically derived regions between Neanderthals and MHs[23]. When limiting the analysis only to DMGs where the most significant DMRs are found (top quartile), the over-representation of voice-affecting genes becomes even more pronounced, with the vocal cords being enriched over 3-fold (FDR = 4.2×10^{-3}), and the larynx over 2-fold (FDR = 6.1×10^{-3}, Fig. 1d, Extended Data Table 4). This enrichment is also apparent when examining patterns of gene expression (Extended Data Table 5). Disease-causing mutations in these voice-affecting genes are associated with various phenotypes, ranging from slight changes of the pitch and hoarseness of the voice, to a complete loss of speech ability (Table 1)[22]. These phenotypes were shown be driven primarily by alterations to the laryngeal skeleton (the cartilaginous structures to which the vocal cords are anchored) and vocal tract (the pharyngeal, oral and nasal cavities, where sound is filtered to specific frequencies). Importantly, the laryngeal skeleton, and particularly the cricoid and arytenoid cartilages that are central in vocalization, are very close developmentally to limb bones, as both of these skeletal tissues derive from the somatic layer of the lateral plate mesoderm. Given that DMRs in one tissue often extend to other tissues[24], it is likely that many of the DMRs identified between limb samples in this study exist in the larynx as well. This is particularly likely in skeletal DMRs, where the differences in methylation are observed across various types of skeletal parts.

Using randomization tests and promoter-specific analyses, we ruled out the possibility that the enrichment of the larynx and face stems from potentially unique characteristics of genes affecting these body parts (such as unique distributions of gene length or genomic position). In addition, we found no enrichment of voice-affecting genes in DMGs along the archaic lineages, nor when reconstructing methylation maps based on simulated data (Extended Data Fig. 1, Extended Data Table 4). Finally, DMRs that separate chimpanzees from all humans (archaic and MH) do not show enrichment for genes that affect the voice, larynx or the vocal tract, compatible with the

bioRxiv preprint doi: https://doi.org/10.1101/106955; this version posted April 5, 2017. The copyright holder for this preprint (which was not certified by peer review) is the author/funder. All rights reserved. No reuse allowed without permission.

notion that this trend emerged only along the MH lineage. We conclude that voice-affecting genes are the most over-represented DMGs along the MH lineage, regardless of intra-skeletal variability, coverage by methylation array probes, the extent to which a DMR is variable across human or chimpanzee populations, or the significance level of the DMRs.

Expansive changes in voice-affecting genes

Our results show that methylation levels in many voice-affecting genes have changed since the split from archaic humans, but they do not provide information on the extent of changes within each gene. To do so, we scanned the genome in windows of 100 kb and computed the fraction of CpGs which are differentially methylated in MHs (hereinafter, MH-derived CpGs). We found that this fraction is more than twice as high within genes affecting the voice compared to other genes (0.142 vs. 0.055, $P = 3.7\text{x}10^{-5}$, *t*-test). Moreover, three of the five DMGs with the highest fraction of MH-derived CpGs affect the laryngeal skeleton[25–28] (*ACAN*, *SOX9* and *COL2A1*; Fig. 2a,b). The fact that so many of the most derived genes affect the larynx is particularly surprising considering that only ~2% of genes (502) are known to affect it.

The extra-cellular matrix (ECM)-related genes *ACAN* and *COL2A1*, and their key regulator *SOX9*, form a network of genes that regulate skeletal growth, pre-ossification processes, and spatio-temporal patterning of skeletal development, including that of the facial and laryngeal skeleton in human[25,26] and mouse[29]. Hypermethylation of the *SOX9* promoter in human was shown to down-regulate its activity, and consequently, its targets[30]. *SOX9* is also regulated by a series of upstream enhancers identified in mouse and human[31]. We show that the *SOX9* promoter, three of its proximal enhancers, including one that is active in mesenchymal cells[31] (covered by DMR #30), as well as the targets of SOX9: *ACAN* (DMR #224) and *COL2A1* (DMR #1, the most significant MH-derived DMR), and an upstream lincRNA (*LINC02097*) , have all become hypermethylated in MHs (Fig. 2c). Additionally, a more distant putative enhancer, located 345kb upstream of *SOX9*, was shown to bear strong active histone modification marks in chimpanzee craniofacial progenitor cells, while in humans these marks are almost absent (~10x stronger in chimpanzee, Fig. 2d)[32]. In human and chimpanzee non-skeletal tissues, however, these genes exhibit very similar methylation patterns. Notably, the amino acid sequence coded by each of these genes is identical in the different human groups[1], suggesting that the changes along the MH lineage are purely regulatory, whereby *SOX9*

bioRxiv preprint doi: https://doi.org/10.1101/106955; this version posted April 5, 2017. The copyright holder for this preprint (which was not certified by peer review) is the author/funder. All rights reserved. No reuse allowed without permission.

became down-regulated in skeletal tissues, followed by hypermethylation and possibly down-regulation of its targets, *ACAN* and *COL2A1* (Fig. 2c).

Effects of down-regulation of *NFIX*

To further explore expression changes driven by changes in methylation, we scanned the DMRs to identify those whose methylation level is strongly correlated with expression. Particularly noteworthy is *NFIX*, one of the most derived genes in MH (ranked #13 in DMR density, Fig. 2b), which controls the balance between lower and upper projection of the face[33]. *NFIX* harbors two skeletal MH-derived DMRs, whose level of DNA methylation explains 73.9% and 81.7% of NFIX expression variation (FDR = 6.2×10^{-3} and 7.5×10^{-4}, Fig. 3a-d). This strong association between *NFIX* methylation and expression was also shown previously[34], and suggests that the hypermethylation reflects down-regulation that emerged along the MH lineage (Fig. 3b). Indeed, we find that *NFIX*, as well as *SOX9, ACAN* and *COL2A1*, show significantly reduced expression levels in humans compared to mice ($P = 0.017$, *t*-test, Extended Data Fig. 2a). Interestingly, NFI proteins were shown to bind the upstream enhancers of *SOX9*[35], hence suggesting a possible mechanism to the simultaneous change in the voice- and face-affecting genes.

To test whether changes in NFIX expression could explain morphological changes in MHs, we examined its skeletal phenotypes. Mutations in *NFIX* were shown to be behind the Marshall-Smith and Malan syndromes, whose phenotypes include various skeletal alterations such as hypoplasia of the midface, retracted lower jaw, and depressed nasal bridge[33], as well as limited speech capabilities[36]. In many cases, the syndromes are driven by heterozygous loss-of-function mutations that could be paralleled to partial silencing, hence suggesting that the phenotypes associated with NFIX are dosage-dependent[33]. Given that reduced activity of *NFIX* drives these symptoms, a simplistic hypothesis would be that increased *NFIX* activity in the Neanderthal would result in changes in the opposite direction. Indeed, we found this to be the case in 18 out of 22 Marshall-Smith syndrome skeletal phenotypes, and in 8 out of 9 Malan syndrome skeletal phenotypes. In other words, from the *NFIX*-related syndromes, through healthy MHs, to the Neanderthal, the level of phenotype manifestation corresponds to the level of *NFIX* activity (Fig. 3c, Extended Data Table 7). Interestingly, many cases of laryngeal malformations in the Marshall-Smith syndrome have been reported[37]. Some of the patients exhibit positional changes of the larynx, changes in its width, and structural alterations to the arytenoid cartilage – the anchor point of the vocal cords, which

bioRxiv preprint doi: https://doi.org/10.1101/106955; this version posted April 5, 2017. The copyright holder for this preprint (which was not certified by peer review) is the author/funder. All rights reserved. No reuse allowed without permission.

controls their movement[37]. In fact, these laryngeal and facial anatomical changes are thought to underlie the limited speech capabilities observed in some patients[36].

Discussion

In light of the role of facial flattening in determining speech capabilities, it is illuminating that flattening of the face is the most common phenotype associated with reduced activity of *SOX9*, *ACAN* and *COL2A1*[22]: Heterozygous loss-of-function mutations in *SOX9*, which result in a reduction of ~50% in its activity, were shown to cause a retracted lower face, and to affect the pitch of the voice[25,26]. *ACAN* was shown to affect facial prognathism and hoarseness of the voice[27]. *COL2A1* is key for proper laryngeal skeletal development[28], and its decreased activity results in a retracted face[38]. One of the key features separating archaic from modern humans is facial retraction. It was shown that the lower and midface of MHs is markedly retracted compared to apes, Australopithecines, and other *Homo* groups[10]. The developmental alterations that underlie the ontogeny of the human face are still under investigation. Cranial base length and flexion were shown to play a role in the retracted face[10], but reduced growth rate, and heterochrony of spatio-temporal switches are thought to be involved as well[39]. Importantly, *SOX9* and *COL2A1* were implemented in the elongation and ossification of the basicranium[40,41], and *SOX9* is a key regulator of skeletal growth rate, and the developmental switch to ossification[25,26].

A limitation in DNA methylation analyses is that some loci differ between cell types and sexes, change with age, and might be affected by factors such as environment, diet, etc. We account for this by combining information from diverse methylation maps. In MH-derived DMRs, for example, we use only DMRs in which chimpanzees and archaic humans form a cluster that is distinct from the cluster of MHs. Both clusters contain samples from females and males, and from a variety of ages and bones (most coming from femurs in both groups, Extended Data Table 1). Therefore, the observed differences are unlikely to be driven by these factors, but rather add credence to the notion that they reflect true MH-specific evolutionary shifts. This is further supported by the phenotypic observations that facial prognathism in general, and facial growth rates in particular, are derived and reduced in MH[42].

We identified the *SOX9*, *ACAN* and *COL2A1* regions as some of the most derived loci in MHs. These genes are active mainly in early stages of osteochondrogenesis, making the observation of differential methylation in mature bones puzzling at first glance. This could be explained by two

bioRxiv preprint doi: https://doi.org/10.1101/106955; this version posted April 5, 2017. The copyright holder for this preprint (which was not certified by peer review) is the author/funder. All rights reserved. No reuse allowed without permission.

factors: (i) The DMRs might reflect earlier changes in the mesenchymal progenitors of these cells that are carried on to later stages of osteogenesis. This is supported by the observation that the upstream mesenchymal enhancer[31] of SOX9 is differentially methylated in MHs (Fig. 2d). (ii) Although these genes are downregulated with the progress towards skeletal maturation, they were shown to be expressed also in later skeletal developmental stages in the larynx, vertebras, limbs, and jaws, including in their osteoblasts[29,43,44]. Interestingly, these are also the organs that are most affected by mutations in these genes[25–28,38].

We have shown here that genes affecting vocal and facial anatomy went through extensive regulatory changes in recent MH evolution. These alterations are observed both in the number of diverged genes and in the extent of changes within each gene, and they are also evident in MH phenotypes. Our results support the notion that the evolution of the vocalization apparatus of MHs is unique among hominins and great apes, and that this evolution was driven, at least partially, by changes in gene regulation.

bioRxiv preprint doi: https://doi.org/10.1101/106955; this version posted April 5, 2017. The copyright holder for this preprint (which was not certified by peer review) is the author/funder. All rights reserved. No reuse allowed without permission.

References

1. Prüfer, K. *et al.* The complete genome sequence of a Neanderthal from the Altai Mountains. *Nature* **505,** 43–9 (2014).

2. Meyer, M. *et al.* A high-coverage genome sequence from an archaic Denisovan individual. *Science* **338,** 222–6 (2012).

3. King, M. C. & Wilson, A. C. Evolution at two levels in humans and chimpanzees. *Science* **188,** 107–116 (1975).

4. Lieberman, P. The Evolution of Human Speech: Its Anatomical and Neural Bases. *Curr. Anthropol.* **48,** 39–66 (2007).

5. Fitch, W. T. The evolution of speech: A comparative review. *Trends in Cognitive Sciences* **4,** 258–267 (2000).

6. Fitch, W. T., de Boer, B., Mathur, N. & Ghazanfar, A. A. Monkey vocal tracts are speech-ready. *Sci. Adv.* **2,** (2016).

7. Lieberman, D. E., McCarthy, R. C., Hiiemae, K. M. & Palmer, J. B. Ontogeny of postnatal hyoid and larynx descent in humans. *Arch. Oral Biol.* **46,** 117–128 (2001).

8. Stevens, K. in *Human Communication A Unified View* 51–66 (1972).

9. De Boer, B. Modelling vocal anatomy's significant effect on speech. *J. Evol. Psychol.* **8,** 351–366 (2010).

10. Lieberman, D. E. *The Evolution of the Human Head*. (Harvard University Press, 2011).

11. Steele, J., Clegg, M. & Martelli, S. Comparative morphology of the hominin and african ape hyoid bone, a possible marker of the evolution of speech. *Hum Biol* **85,** 639–672 (2013).

12. Lieberman P. and McCarthy C. The Evolution of Speech and Language. *Handb. Paleoanthropology* (2014).

13. Gokhman, D. *et al.* Reconstructing the DNA methylation maps of the Neandertal and the Denisovan. *Science* **344,** 523–527 (2014).

14. Briggs, A. W. *et al.* Removal of deaminated cytosines and detection of in vivo methylation in ancient DNA. *Nucleic Acids Res.* **38,** (2010).

bioRxiv preprint doi: https://doi.org/10.1101/106955; this version posted April 5, 2017. The copyright holder for this preprint (which was not certified by peer review) is the author/funder. All rights reserved. No reuse allowed without permission.

15. Pedersen, J. S. *et al.* Genome-wide nucleosome map and cytosine methylation levels of an ancient human genome. *Genome Res.* **24,** 454–466 (2014).

16. Fu, Q. *et al.* Genome sequence of a 45,000-year-old modern human from western Siberia. *Nature* **514,** 445–9 (2014).

17. Lazaridis, I. *et al.* Ancient human genomes suggest three ancestral populations for present-day Europeans. *Nature* **513,** 409–413 (2014).

18. Olalde, I. *et al.* Derived immune and ancestral pigmentation alleles in a 7,000-year-old Mesolithic European. *Nature* **507,** 225–228 (2014).

19. Wang, H. *et al.* Widespread plasticity in CTCF occupancy linked to DNA methylation. *Genome Res.* **22,** 1680–1688 (2012).

20. Horvath, S. *et al.* The cerebellum ages slowly according to the epigenetic clock. *Aging (Albany. NY).* **7,** 294–306 (2015).

21. Lokk, K. *et al.* DNA methylome profiling of human tissues identifies global and tissue-specific methylation patterns. *Genome Biol.* **15,** r54 (2014).

22. Gokhman, D. *et al.* Gene ORGANizer: Linking Genes to the Organs They Affect. *BioXkiv* (2017). doi:https://doi.org/10.1101/106948

23. Weaver, T. D. The meaning of Neandertal skeletal morphology. *Proc. Natl. Acad. Sci.* **106,** 16028–16033 (2009).

24. Irene Hernando-Herraez, Holger Heyn, Marcos Fernandez-Callejo, Enrique Vidal, Hugo Fernandez-Bellon, Javier Prado-Martinez, Andrew J. Sharp, Manel Esteller, and T. M.-B. The interplay between DNA methylation and sequence divergence in recent human evolution. *Nucleic Acids Res.* **43,** 8204–8214 (2015).

25. Meyer, J. *et al.* Mutational analysis of the SOX9 gene in campomelic dysplasia and autosomal sex reversal: Lack of genotype/phenotype correlations. *Hum. Mol. Genet.* **6,** 91–98 (1997).

26. Lee, Y. H. & Saint-Jeannet, J. P. Sox9 function in craniofacial development and disease. *Genesis* **49,** 200–208 (2011).

27. Tompson, S. W. *et al.* A Recessive Skeletal Dysplasia, SEMD Aggrecan Type, Results from a Missense Mutation Affecting the C-Type Lectin Domain of Aggrecan. *Am. J. Hum. Genet.* **84,** 72–

bioRxiv preprint doi: https://doi.org/10.1101/106955; this version posted April 5, 2017. The copyright holder for this preprint (which was not certified by peer review) is the author/funder. All rights reserved. No reuse allowed without permission.

79 (2009).

28. Frenzel, K., Amann, G. & Lubec, B. Deficiency of laryngeal collagen type II in an infant with respiratory problems. *Arch. Dis. Child.* **78,** 557–9 (1998).

29. Ng, L. J. *et al.* Sox9 binds DNA, activates transcription, and coexpresses with type II collagen during chondrogenesis in the mouse. *Dev. Biol.* **183,** 108–121 (1997).

30. Kim, K. Il, Park, Y. S. & Im, G. Il. Changes in the epigenetic status of the SOX-9 promoter in human osteoarthritic cartilage. *J. Bone Miner. Res.* **28,** 1050–1060 (2013).

31. Yao, B. *et al.* The SOX9 upstream region prone to chromosomal aberrations causing campomelic dysplasia contains multiple cartilage enhancers. *Nucleic Acids Res.* **43,** 5394–5408 (2015).

32. Prescott, S. L. *et al.* Enhancer Divergence and cis-Regulatory Evolution in the Human and Chimp Neural Crest. *Cell* **163,** 68–84 (2015).

33. Malan, V. *et al.* Distinct effects of allelic NFIX mutations on nonsense-mediated mRNA decay engender either a sotos-like or a Marshall-Smith Syndrome. *Am. J. Hum. Genet.* **87,** 189–198 (2010).

34. Carrió, E. *et al.* Deconstruction of DNA methylation patterns during myogenesis reveals specific epigenetic events in the establishment of the skeletal muscle lineage. *Stem Cells* **33,** 2025–2036 (2015).

35. Pjanic, M. *et al.* Nuclear Factor I genomic binding associates with chromatin boundaries. *BMC Genomics* **14,** 99 (2013).

36. Shaw, A. C. *et al.* Phenotype and natural history in Marshall-Smith syndrome. *Am. J. Med. Genet. Part A* **152,** 2714–2726 (2010).

37. A. Cullen á T. A. Clarke á T. P. O'Dwyer. The Marshall-Smith syndrome: a review of the laryngeal complications. *Eur J Pediatr* **156,** 463–464 (1997).

38. Hoornaert, K. P. *et al.* Stickler syndrome caused by COL2A1 mutations: genotype–phenotype correlation in a series of 100 patients. *Eur J Hum Genet.* **18,** 872–880 (2010).

39. Bastir, M., O'Higgins, P. & Rosas, A. Facial ontogeny in Neanderthals and modern humans. *Proc. R. Soc. B Biol. Sci.* **274,** 1125–1132 (2007).

40. Horton WA, Rimoin DL, Hollister DW, L. R. Further heterogeneity within lethal neonatal short-limbed dwarfism: the platyspondylic types. *J Pediatr.* **94,** 736–42 (1979).

bioRxiv preprint doi: https://doi.org/10.1101/106955; this version posted April 5, 2017. The copyright holder for this preprint (which was not certified by peer review) is the author/funder. All rights reserved. No reuse allowed without permission.

41. Yan, Y.-L. *et al.* A pair of Sox: distinct and overlapping functions of zebrafish sox9 co-orthologs in craniofacial and pectoral fin development. *Development* **132,** 1069–1083 (2005).

42. Lacruz, R. S. *et al.* Ontogeny of the maxilla in Neanderthals and their ancestors. *Nat. Commun.* **6,** 8996 (2015).

43. Rojas-Peña, M. L. *et al.* Characterization of distinct classes of differential gene expression in osteoblast cultures from non-syndromic craniosynostosis bone. *J. genomics* **2,** 121–30 (2014).

44. Moriarity, B. S. *et al.* A Sleeping Beauty forward genetic screen identifies new genes and pathways driving osteosarcoma development and metastasis. *Nat. Genet.* **47,** 615–24 (2015).

bioRxiv preprint doi: https://doi.org/10.1101/106955; this version posted April 5, 2017. The copyright holder for this preprint (which was not certified by peer review) is the author/funder. All rights reserved. No reuse allowed without permission.

Acknowledgements

We would like to thank Sagiv Shifman, Yoel Rak, Philip Lieberman, Rodrigo Lacruz, Erella Hovers, Anna Belfer-Cohen, Achinoam Blau, and Daniel Lieberman for their useful advice, Nadin Rohland for helping with the sequencing of the La Braña 1 individual, Janet Kelso for providing data, and Maayan Harel for illustrations. L.C and E.M are supported by the Israel Science Foundation FIRST individual grant (ISF 1430/13). S.P. and K.P. were supported by ERC grant (No 694707) and the Max Planck Society. C.L.-F. is supported by FEDER and BFU2015-64699-P grant from the Spanish government. Funding for the collection and processing of the 850K chimp data was provided by the Leakey Foundation Research Grant for Doctoral Students, Wenner-Gren Foundation Dissertation Fieldwork Grant (Gr. 9310), James F. Nacey Fellowship from the Nacey Maggioncalda Foundation, International Primatological Society Research Grant, Sigma Xi Grant-in-Aid of Research, Center for Evolution and Medicine Venture Fund (ASU), Graduate Research and Support Program Grant (GPSA, ASU), and Graduate Student Research Grant (SHESC, ASU) to G.H. Collection of the chimpanzee bone from Tanzania was funded by the Jane Goodall Institute, and grants from the US National Institutes of Health (AI 058715) and National Science Foundation (IOS-1052693), and facilitated by Elizabeth Lonsdorf and Beatrice Hahn.

bioRxiv preprint doi: https://doi.org/10.1101/106955; this version posted April 5, 2017. The copyright holder for this preprint (which was not certified by peer review) is the author/funder. All rights reserved. No reuse allowed without permission.

Tables and Figures

Table 1. DMGs that affect the voice and the larynx.

DMG	Associated phenotype	Chr	DMR start	DMR end
ALPL	Abnormality of the voice	1	21901961	21907487
AHDC1	Laryngomalacia	1	27869253	27871400
AHDC1	Laryngomalacia	1	27917471	27921806
SATB2	Abnormality of the voice	2	200236735	200244763
SPEG	Dysphonia	2	220316303	220319764
COLQ	Weak cry	3	15508914	15512536
TGFBR2	Abnormality of the voice	3	30649533	30658854
TGFBR2	Abnormality of the voice	3	30674279	30680742
TGFBR2	Abnormality of the voice	3	30706167	30710950
POC1A	High pitched voice	3	52110680	52112683
PLXND1	Abnormality of the voice	3	129312022	129315078
SH3BP2	Abnormality of the voice	4	2796208	2800983
SDHA	Hoarse voice, loss of voice, vocal cord paralysis	5	251676	254993
GLI3	Laryngeal cleft	7	42212811	42214593
CHD7	Abnormality of the voice, Laryngomalacia	8	61679558	61684133
HNRNPA1	Bowing of the vocal cords, hoarse voice	12	54679251	54682731
TRPV4	Vocal cord paresis	12	110248589	110250088
MEIS2	Laryngomalacia	15	37217518	37219852
ACAN	Hoarse voice	15	89333945	89344957
CREBBP	Laryngomalacia	16	3828787	3834862
CREBBP	Laryngomalacia	16	3891316	3900883
XYLT1	High-pitched voice	16	17428938	17431410
WWOX	Abnormality of the voice	16	78707061	78709972
WWOX	Abnormality of the voice	16	79038137	79040340
SOX9	Laryngomalacia	17	70077734	70113643
SOX9	Laryngomalacia	17	70119247	70120418
GNAL	Laryngeal dystonia	18	11747116	11748993
NFIX	Laryngomalacia	19	13155588	13158871
NFIX	Laryngomalacia	19	13185658	13192650
POLD1	High-pitched voice	19	50883926	50885758
RIN2	High-pitched voice	20	19944783	19947262
TBX1	Abnormality of the voice, nasal speech	22	19748985	19750495

bioRxiv preprint doi: https://doi.org/10.1101/106955; this version posted April 5, 2017. The copyright holder for this preprint (which was not certified by peer review) is the author/funder. All rights reserved. No reuse allowed without permission.

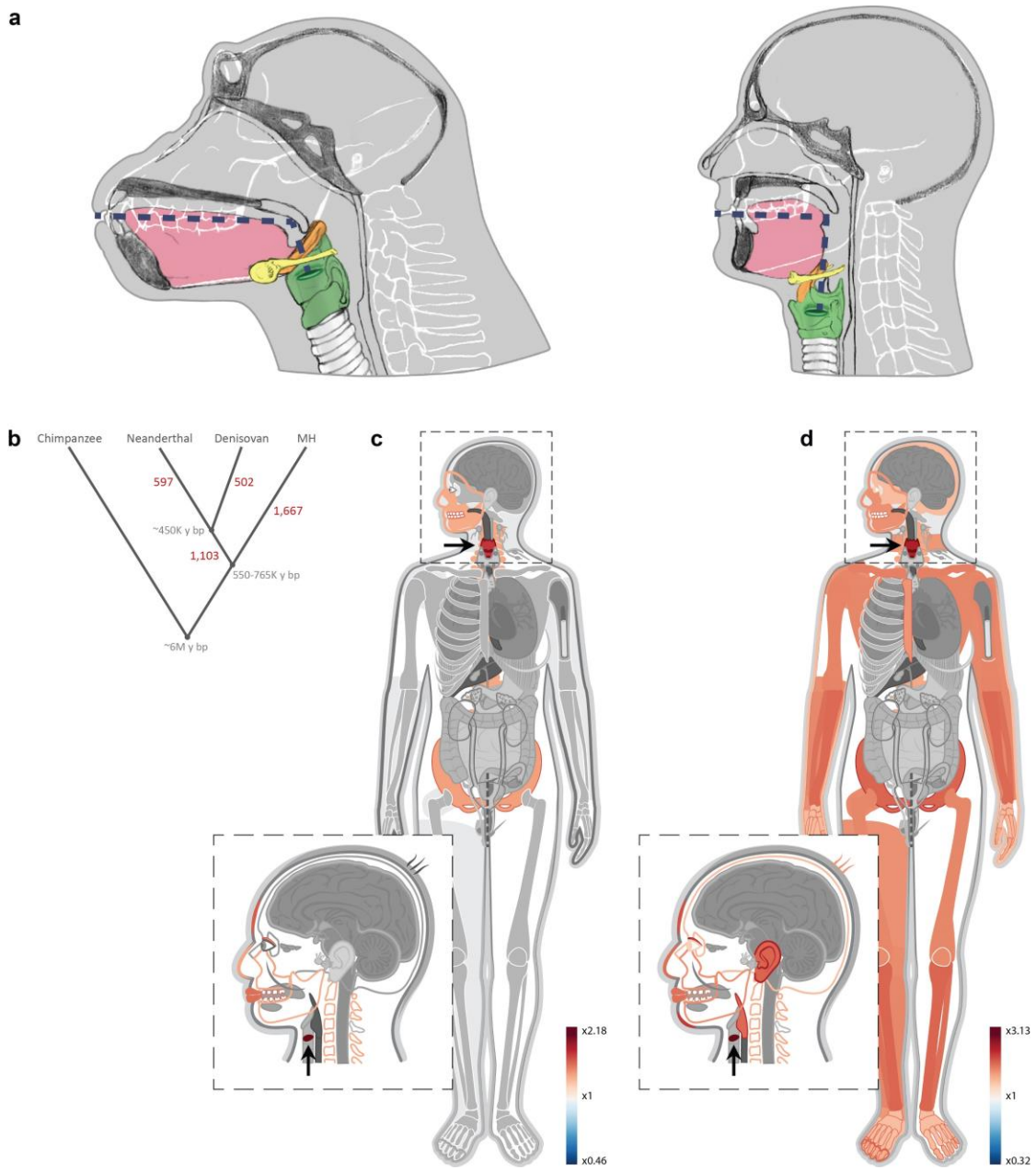

Fig. 1. Genes affecting the voice are the most over-represented within MH-derived DMRs. a. Vocal anatomy of chimpanzee and MH. Colors mark central body parts: larynx and vocal cords (green), epiglottis (orange), hyoid bone (yellow), and tongue (pink). The vocal tract is the cavity from the lips to the larynx. In MHs, the flattening of the face together with the descent of the larynx (marked by dashed blue lines), led to approximately 1:1 proportions of the horizontal and vertical portions of the vocal tract, whereas chimpanzees have a longer horizontal and a shorter vertical vocal tract. **b.** The number of DMRs that emerged along each of the human branches. Split times are in years before present (ybp). **c.** A heat map representing the level of enrichment of each anatomical part within the skeletal MH-derived DMRs. Only body parts that are significantly enriched (FDR < 0.05) are colored. Most enriched parts are within the head and neck region, with the vocal cords and voice box (larynx, marked with arrows) being the most

bioRxiv preprint doi: https://doi.org/10.1101/106955; this version posted April 5, 2017. The copyright holder for this preprint (which was not certified by peer review) is the author/funder. All rights reserved. No reuse allowed without permission.

over-represented. **d.** Enrichment levels of the most significant (first quartile) skeletal MH-derived DMRs, showing an even more pronounced over-representation of genes affecting vocal anatomy.

bioRxiv preprint doi: https://doi.org/10.1101/106955; this version posted April 5, 2017. The copyright holder for this preprint (which was not certified by peer review) is the author/funder. All rights reserved. No reuse allowed without permission.

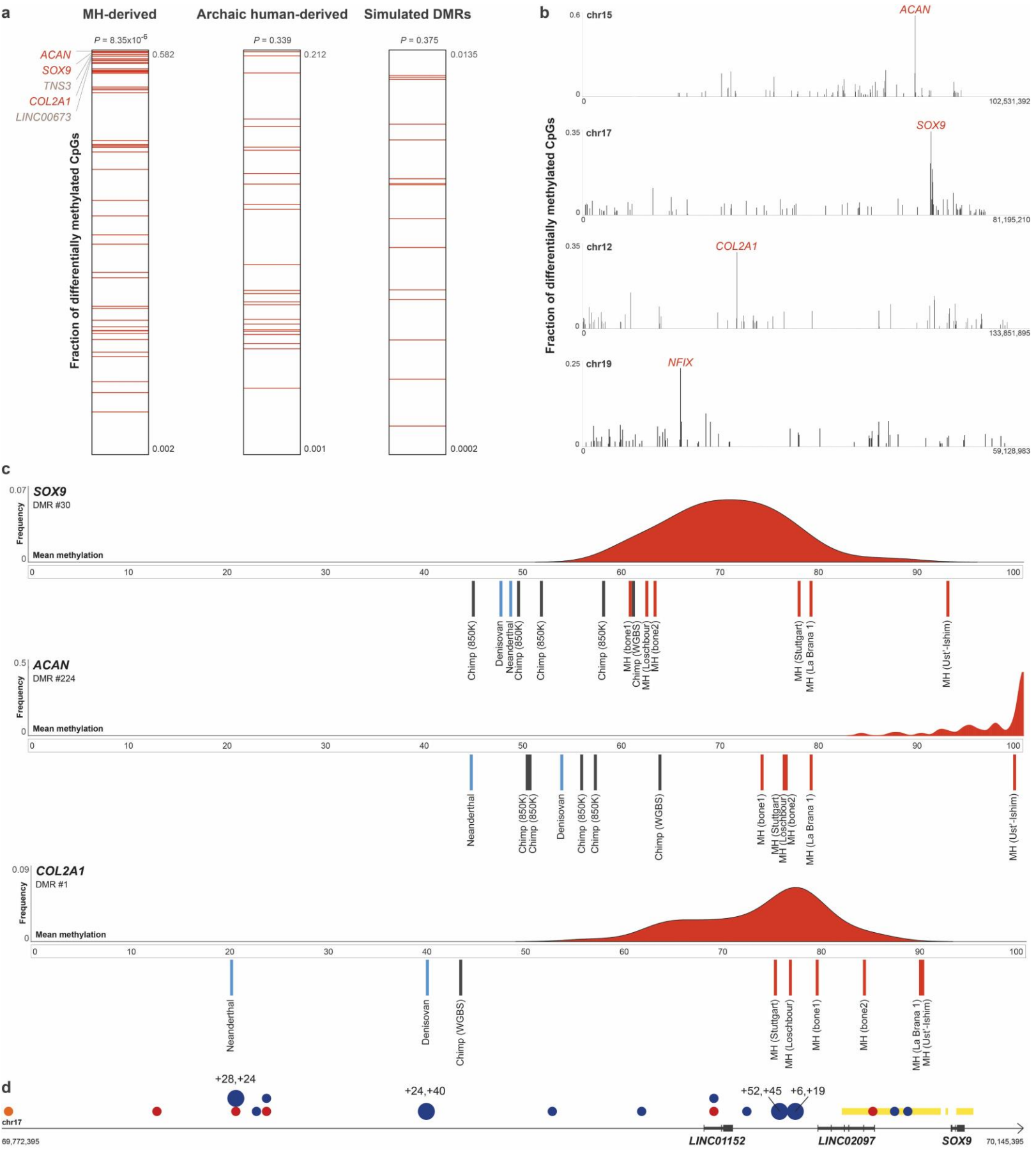

bioRxiv preprint doi: https://doi.org/10.1101/106955; this version posted April 5, 2017. The copyright holder for this preprint (which was not certified by peer review) is the author/funder. All rights reserved. No reuse allowed without permission.

Fig. 2. The extent of differential methylation in MHs is highest among genes affecting the larynx. a. The number of MH-derived CpGs per 100 kb centered around the middle of each DMR. Genes were ranked according to the fraction of derived CpG positions within them. Genes affecting the voice are marked with red lines. In MH-derived DMGs, these genes went through more extensive changes compared to other genes, and tend to be ranked higher. Although these genes comprise ~2% of the genome, three of the top five MH-derived windows overlap genes affecting the voice. In archaic-derived DMRs and in simulated DMRs, voice-affecting genes do not harbor more changes compared to the rest of the genome. **b.** The fraction of MH-derived CpGs along the four chromosomes containing *ACAN*, *SOX9*, *COL2A1* and *NFIX*. The most extensive changes are found within the genes *COL2A1*, *SOX9*, *ACAN*, and *NFIX*. All of these genes control facial projection and the development of the larynx. **c.** Methylation levels in the skeletal MH-derived DMRs in *SOX9*, *ACAN* and *COL2A1*. MH samples are marked with red lines, archaic human samples are marked with blue lines and chimpanzee samples are marked with grey lines. The distribution of methylation across 52 MH samples (450K methylation arrays) is presented as a red distribution. **d.** *SOX9* and its upstream regulatory elements. MH-derived DMRs are marked with yellow rectangles, enhancers identified in humans are marked with red dots, enhancers identified in mice are marked with blue dots, enhancers which were shown to be active in skeletal tissues (mainly cartilage) are marked with large dots, and a putative enhancer that bears active histone marks in chimpanzee, but not in modern humans is marked with an orange dot. Numbers above skeletal enhancers show mean MH methylation levels compared to mean archaic methylation (1st number) and chimpanzee methylation (2nd number) in full bone methylomes. Across all four enhancers, MHs are hypermethylated compared to archaic humans and the chimpanzee.

bioRxiv preprint doi: https://doi.org/10.1101/106955; this version posted April 5, 2017. The copyright holder for this preprint (which was not certified by peer review) is the author/funder. All rights reserved. No reuse allowed without permission.

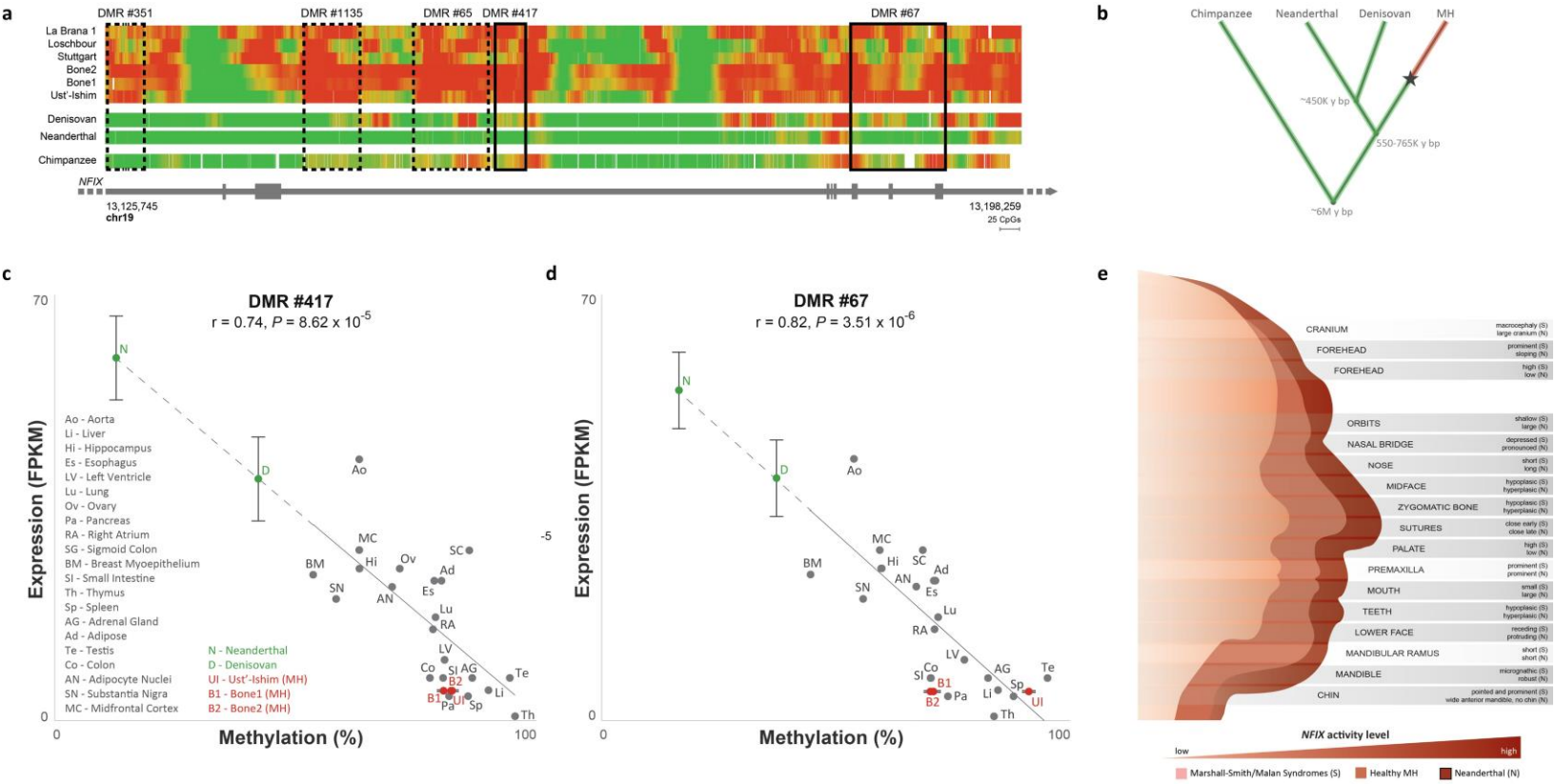

Fig. 3. *NFIX* became down-regulated after the split from archaic humans, and possibly underlies the flattening of the face in MHs. a. Methylation levels along *NFIX*, color-coded from green (unmethylated) to red (methylated). The top six panels show ancient and present-day MH samples, where *NFIX* is mostly methylated. The bottom three panels describe the Denisovan, Neanderthal and chimpanzee, where the gene is mostly unmethylated. Full bone MH-derived DMRs are shown in dashed rectangles, skeletal MH-derived DMRs are shown in plain rectangles. Chimpanzee and present-day samples were smoothed using the same sliding window as in ancient samples to allow easier comparison. **b.** The inferred schematic regulatory evolution of *NFIX*, showing when the shift in the NFIX DMRs from unmethylated (green) to methylated (red) had occurred. **c,d**. Methylation levels in DMRs #417 and #67 vs. expression levels of *NFIX* across 21 MH tissues (grey). In both DMRs, higher methylation is associated with lower expression of *NFIX*. Ust'-Ishim, Bone1 and Bone2 methylation levels (red) are plotted against mean NFIX expression from four present-day bones. Neanderthal and Denisovan methylation levels are plotted against the predicted expression levels, based on the extrapolated regression line (dashed). Error bars represent one standard deviation in each direction. **e**. Craniofacial features of the Neanderthal, healthy MH, and MH with Marshall-Smith or Malan syndromes. *NFIX* controls the upper vs. lower prognathism of the face. Individuals where *NFIX* is partially or completely inactive present phenotypes that are largely the opposite of the Neanderthal facial features. For each facial part we show the phenotype of the Marshall-Smith and Malan syndromes (S), as well as the corresponding Neanderthal (N) phenotype. Phenotypes are compared to a healthy MH. Opposite phenotypes are marked with dark grey rectangles, and shared phenotypes are marked with light grey rectangles.

bioRxiv preprint doi: https://doi.org/10.1101/106955; this version posted April 5, 2017. The copyright holder for this preprint (which was not certified by peer review) is the author/funder. All rights reserved. No reuse allowed without permission.

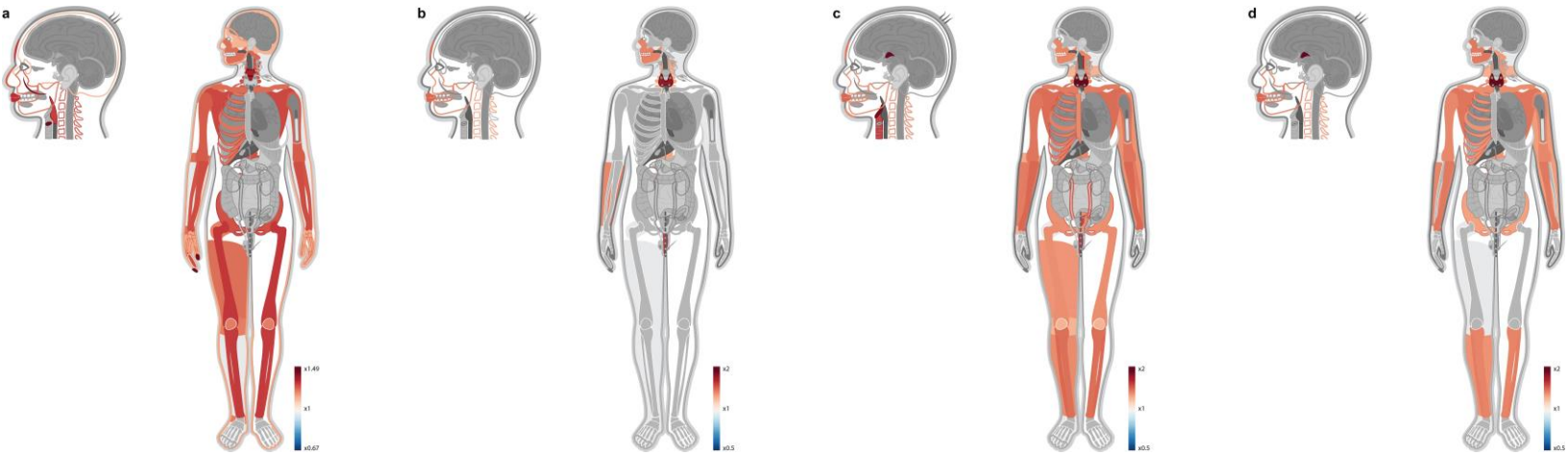

Extended Data Fig. 1. Genes affecting endocrine glands and the skeleton are the most enriched within archaic-derived DMRs. A heat map representing the level of enrichment of each anatomical part within archaic-derived DMGs. Only body parts that are significantly enriched (FDR < 0.05) are colored. **a.** Enrichment within full bone MH-derived DMRs. **b.** Enrichment within full bone archaic-derived DMRs. **c.** Enrichment within bone archaic-derived DMRs. **d.** Enrichment within skeletal archaic-derived DMRs.

bioRxiv preprint doi: https://doi.org/10.1101/106955; this version posted April 5, 2017. The copyright holder for this preprint (which was not certified by peer review) is the author/funder. All rights reserved. No reuse allowed without permission.

bioRxiv preprint doi: https://doi.org/10.1101/106955; this version posted April 5, 2017. The copyright holder for this preprint (which was not certified by peer review) is the author/funder. All rights reserved. No reuse allowed without permission.

Extended Data Fig. 2. a. Expression levels of *SOX9*, *ACAN*, *COL2A1* and *NFIX* in humans are reduced compared to mice. Box plot presenting 89 human samples and four mouse samples from appendicular bones (limbs and pelvis). Expression levels were converted to percentiles, based on the level of gene expression compared to the rest of the genome in each sample. Green and red box plots represent mouse and human samples, respectively. **b.** The procedure of merging overlapping DMRs. Plain red lines represent overlapping regions. Dashed red lines represent regions that were identified as a DMR in one of the lists, but not the other. These regions were added to the overlapping region if they clustered significantly closer to the reference human. **c.** Simulations of cytosine deamination, followed by reconstruction reproduce DNA methylation maps. Deamination was simulated for each position based on its methylation level, read coverage and the observed rate of deamination in each hominin. Then, DNA methylation maps were reconstructed and matched against the original map. The number of DMRs found were used as an estimate of false discovery rate. Three exemplary regions are presented. **d.** The HOXD cluster is hypermethylated in archaic humans, and in the Ust'-Ishim individual. Methylation levels are color-coded from green (unmethylated) to red (methylated). The top seven panels show ancient and present-day MH samples, the lower three show the Denisovan, Neanderthal and chimpanzee. The promoter region of *HOXD9* is hypermethylated in the Neanderthal and the Denisovan, but not in MHs. The 3' ends of the three genes are hypermethylated in the Neanderthal, Denisovan, Ust'-Ishim and chimpanzee, but not in other MH samples. The promoter of HOXD10 is methylated only in the Denisovan. **e.** *COL2A1, ACAN, SOX9,* and *NFIX* are hypermethylated in MH femurs compared to chimpanzee femurs. Each dot represents a methylation array probe. Even when comparing methylation in the same bone, measured by the same technology, and across the same positions, MHs show consistent hypermethylation in these genes. **f.** *COL2A1, ACAN, SOX9,* and *NFIX* are hypermethylated in Ust'-Ishim compared to the Vindija Neanderthal. Dots represent mean methylation levels in MH-derived DMRs. Both samples were extracted from femurs of adults, and methylation was reconstructed using the same method. Therefore, the hypermethylation of these genes in MHs is unlikely to be attributed to age or bone type.